Development of MgO concrete with enhanced hydration and carbonation mechanisms

Dung, N.T.; Unluer, C.

2018

Dung, N., & Unluer, C. (2018). Development of MgO concrete with enhanced hydration and carbonation mechanisms. Cement and Concrete Research, 103, 160-169.

https://hdl.handle.net/10356/85800

https://doi.org/10.1016/j.cemconres.2017.10.011

Development of MgO concrete with enhanced hydration and carbonation mechanisms

N.T. Dung[a], C. Unluer[a,*]

[a] School of Civil and Environmental Engineering, Nanyang Technological University, 50 Nanyang Avenue, Singapore 639798

* Corresponding author. Tel.: +65 91964970, E-mail address: ucise@ntu.edu.sg

Abstract

This study proposed the use of hydration agent (HA) and seeds to improve the hydration and carbonation of reactive magnesium cement (RMC)-based concrete formulations. Hydration of RMC was evaluated by isothermal calorimetry. Water absorption and compressive strength results were used to assess the mechanical performance of RMC-based concrete samples. Quantification of hydrate and carbonate phases was performed via XRD and TGA. Formation and morphology of carbonates were observed via BSE and SEM. In addition to increasing the utilization of RMC in the carbonation reaction and facilitating early strength development, the use of HA formed large carbonate phases, while the addition of seeds improved sample microstructures via the development of dense carbonate networks. The improvements in morphology, microstructure and carbonate content in samples involving the simultaneous use of HA and seeds resulted in 56% lower water absorption values and 46% higher 28-day compressive strengths (70MPa) in comparison to the control sample.

Keywords: MgO (D); Hydration (A); Carbonation (C); Compressive strength (C); Microstructure (B)

1 Introduction

Reactive magnesium oxide (MgO), produced at much lower calcination temperatures than PC (i.e. 700-1000 vs. 1450 °C) [1, 2] is a promising material for the sequestration of CO_2 within construction products. The sequestration of CO_2 in reactive MgO cement (RMC) involves the diffusion and dissolving of CO_2 in the pore space, followed by its reaction with Mg-phases to form a range of hydrated magnesium carbonates (HMCs). Some of the main HMCs that have been observed to provide physical strength in RMC formulations are needle-like nesquehonite ($MgCO_3 \cdot 3H_2O$), rosette-like hydromagnesite ($4MgCO_3 \cdot Mg(OH)_2 \cdot 4H_2O$) and dypingite ($4MgCO_3 \cdot Mg(OH)_2 \cdot 5H_2O$), and acicular artinite ($MgCO_3 \cdot Mg(OH)_2 \cdot 3H_2O$) [3, 4]. The formation of HMCs is primarily responsible for the strength gain of RMC-based formulations by enabling an increase in density as the formation of carbonate phases reduces the overall pore volume. The carbonation reaction also improves the microstructure and increases strength as the morphology and binding strength of the carbonate crystals contribute to the network structure.

Hydration and carbonation reactions are critical for the strength development of RMC samples as they control the degree of HMC formation [5]. The hydration mechanism of MgO involves a dissolution–precipitation process initially controlled by the dissolution of MgO [6]. However, the hydration degree of MgO is quite low under ambient conditions due to its low rate and degree of dissolution [7-12] and the precipitation of hydration and carbonation products on the surface of unhydrated MgO particles, thereby inhibiting further hydration. The precipitation of carbonate phases on unhydrated $Mg(OH)_{2(aq,s)}$ can also prevent the progress of the carbonation reaction. These limitations in the hydration and carbonation of

RMC can result in its inefficient use as a binder and limit the strength development of concrete formulations it is incorporated in.

Overcoming the limitations associated with the low dissolution of MgO and the subsequent hydration and carbonation reactions can not only increase the formation of HMCs but also improve the mechanical performance of RMC-based concrete formulations. Two methods that can alleviate these challenges include (i) the use of a hydration agent (HA) to improve the dissolution of MgO and increase the amount of $Mg(OH)_{2(aq,s)}$ available for carbonation and (ii) the provision of additional nucleation sites dispersed into the sample pore space to facilitate continuous hydration and carbonation by increasing the surface area for the nucleation and growth of carbonate phases away from the unhydrated MgO and uncarbonated $Mg(OH)_2$.

One of the most effective HAs reported in literature is magnesium acetate ($(CH_3COO)_2Mg$) [13, 14]. The hydration of MgO in the presence of $(CH_3COO)_2Mg$ takes place in a similar mechanism as shown in Equations 1-4. The complex magnesium acetate ions (CH_3COOMg^+) shown in Equation 2 migrate away from their original particles [13] to enable the precipitation of a bulk $Mg(OH)_2$ structure in the spore space. Furthermore, the presence of $Mg^{2+}_{(aq)}$ (Equation 1) promotes the precipitation of $Mg(OH)_2$, whereas $CH_3COO^-_{(aq)}$ facilitates the dissolution of unhydrated MgO. When coupled with the use of HAs, the introduction of additional nucleation sites stimulates the formation of $Mg(OH)_2$ away from the MgO grains. The dispersion of $Mg(OH)_{2(aq,s)}$ into the pore space increases the contact surface area of MgO and $Mg(OH)_{2(aq,s)}$ with water and CO_2, thereby enhancing the hydration and carbonation reactions. These advancements can lead to increased formation of HMCs and therefore improve the mechanical performance of RMC formulations.

Dissociation of magnesium acetate:

$$(CH_3COO)_2Mg_{(aq)} \leftrightarrow 2CH_3COO^-_{(aq)} + Mg^{2+}_{(aq)} \quad (1)$$

Dissolution of magnesia:

$$MgO_{(s)} + CH_3COO^-_{(aq)} + H_2O_{(l)} \leftrightarrow CH_3COOMg^+_{(aq)} + 2OH^-_{(aq)} \quad (2)$$

Dissociation of magnesium complexes:

$$CH_3COOMg^+_{(aq)} \rightarrow CH_3COO^-_{(aq)} + Mg^{2+}_{(aq)} \quad (3)$$

Precipitation of magnesium hydroxide due to supersaturation:

$$Mg^{2+}_{(aq)} + 2OH^-_{(aq)} \rightarrow Mg(OH)_{2(s)} \quad (4)$$

Differing from previous studies that looked into the incorporation of carbonates within RMC systems, which generally led to a decrease in strength due to the high inclusion levels of carbonates (i.e. up to 50% of the cement content) [15], this study involves the use of small amount of carbonate seeds (i.e. up to 1% of the cement content) to improve the reaction mechanisms. The provision of additional nucleation sites via the introduction of seeds (e.g. C-S-H) has been reported to accelerate the nucleation and growth controlled early age hydration in PC [16] and alkali-activated slag [17] systems. This improvement was reflected

as an increase in the compressive strength values of seeded samples, which were up to 5 times higher than those of unseeded samples at early ages [17].

The role of HA in promoting the formation of $Mg(OH)_{2(s)}$ (brucite), rather than HMCs, was demonstrated in previous studies [13, 14]. Differing from PC and alkali-activated systems, whose hydration is limited by the nucleation and growth mechanism, the rate-limiting step in the hydration of MgO systems is the dissolution of MgO. Therefore, while the introduction of seeds in the mix design is beneficial in accelerating the hydration of PC and alkali-activated mixes, this approach does not have the same influence on the early hydration rate of MgO [17]. Alternatively, as the strength gain mechanism of MgO systems mainly rely on the degree of carbonation, the introduction of seeds can increase the overall extent of carbonation by increasing the reactive contact surface within the pore space, thereby facilitating the increased formation of carbonate phases. This led to the simultaneous inclusion of HA and seeds in the mixes prepared in this study, which were aimed to enhance the mechanical performance of RMC samples by increasing the degree of hydration and carbonation, respectively.

The presented approach did not only aim to provide increased hydration, but also to stimulate the carbonation reaction throughout the curing process, the combination of which has not been tackled simultaneously in detail in previous studies. In this respect, a comprehensive analysis on the performance and microstructural development of carbonated RMC concrete formulations involving the use of HA and nucleation seeding was presented. Concrete samples with and without HA were prepared with different seed contents and subjected to carbonation curing for up to 28 days. The influence of these additives on the hydration kinetics of MgO was evaluated by isothermal calorimetry. The performance of the prepared

formulations was analyzed at different durations by compressive strength testing and water absorption measurements. X-ray diffraction (XRD), thermogravimetric analysis (TGA), backscattered electron (BSE) and scanning electron microscopy (SEM) were employed to analyze the formation of hydration and carbonation products and investigate the microstructural development at the end of the curing process.

2 Materials and Methodology

2.1 Materials

The main cement binder used in this study was RMC (commercial name "calcined magnesite 92/200") obtained from Richard Baker Harrison (UK), that was produced at around 1000 °C. The chemical and physical properties of RMC are shown in Table 1. The reactivity of RMC (i.e. measured by the time required for the neutralization of 0.25 M of acetic acid by 5 grams of RMC [18]) was recorded as 520 seconds. Magnesium acetate ($(CH_3COO)_2Mg$), obtained from VWR (Singapore), was used as the HA at a concentration of 0.05 M (i.e. based on previous research [13, 14] and preliminary studies) to promote the hydration process. Hydromagnesite ($4MgCO_3 \cdot Mg(OH)_2 \cdot 4H_2O$) seeds, obtained from Fisher Scientific (UK) with a specific surface area of 43.5 m^2/g, were used to provide additional nucleation sites and stimulate the nucleation and growth of HMCs in the pore space. Fig. 1 shows the microstructure of hydromagnesite seeds, which are spherical agglomerations with a diameter of ~1-7 μm, composed of ~0.5 μm diameter disks. Saturated surface dry (SSD) gravel with a particle size of 4.7–9.5 mm was used to form the aggregate profile in the prepared concrete samples.

2.2 Methodology

Two sets of samples (i.e. with and without HA) were used to investigate the influence of HA and seeding on the hydration and carbonation of RMC formulations. Table 2 lists the compositions of the concrete samples prepared under this study. Each set included seed contents of 0% (samples H_2O.S0 and HA.S0), 0.5% (samples H_2O.S0.5 and HA.S0.5) and 1% (samples H_2O.S1.0 and HA.S1.0) of the total binder content. The ratio of water or HA solution to binder was kept constant at 0.7 for all samples. Before casting the concrete samples, corresponding pastes were prepared to study the effects of HA and seeding on the hydration of MgO via isothermal calorimetry.

To prepare the concrete samples, seeds were dispersed in water/HA solution by a magnetic stirrer and were then added to the dry mix as a part of the mixing solution. The concrete compositions prepared in this study did not include any fine aggregates to enable the extraction of carbonated paste from the concrete samples without any contamination and to ensure accurate quantification of the hydrate and carbonate phases via XRD and TGA. After mixing, the concrete samples were cast into 50×50×50 mm cubic molds, consolidated by a vibrating table and trowel finished. All samples were demoulded after 24 hours and subjected to carbonation curing under 10% CO_2, 80±5% relative humidity and 30±1.5 ^oC for up to 28 days for water absorption and compressive strength measurements, as well as microstructural analysis.

2.2.1 Isothermal calorimetry

The heat flow due to the hydration of each mixture was studied at 30 °C by an I-Cal 8000 High Precision Calorimeter in accordance with ASTM C1702 − 15a [19]. The preparation of pastes involved the dispersion of seeds in H_2O or HA, which was previously heated to 30 °C in order to produce mixes at the same temperature as the measurement temperature. The seeded solution was then mixed with RMC. After around 15-20 seconds of mixing, the prepared pastes were placed into the isothermal calorimeter channel to measure the heat of hydration.

2.2.2 Water absorption

The water absorption of each sample was measured after 14 and 28 days of carbonation. The initial mass of samples was recorded before they were immersed in a water tank. Their absorption mass was also measured when they reached a constant mass under water, which reflected their water absorption capacity. Water absorption (W_{ab}) was calculated as a percentage of the initial mass as shown in Equation 5, where m_{ab} is the absorption mass of samples after reaching a constant mass when immersed in water and m_i is the initial mass.

$$W_{ab} = (m_{ab} - m_i)/m_i \ (\%) \quad (5)$$

2.2.3 Compressive strength

The compressive strength of concrete samples was measured by uni-axial loading in triplicates at 3, 7, 14 and 28 days. The equipment used for this purpose was a Toni Technik Baustoffprüfsysteme machine, operated at a loading rate of 55 kN/min.

2.2.4 XRD, TGA, SEM and BSE analyses

Samples extracted from the cubes crushed during strength testing were stored in acetone for at least 7 days to stop hydration, followed by vacuum drying for another 7 days in preparation for XRD, TGA, SEM and BSE analyses. The vacuum dried samples were ground down to pass through a 75 μm sieve before they were analyzed under XRD and TGA.

XRD was recorded on a Philips PW 1800 spectrometer using Cu K_α radiation (40 kV, 30 mA) with a scanning rate of 0.04° 2θ/step from 5 to 80° 2θ. The Reference Intensity Ratio (RIR) technique [20-22], which provides a comparison of the integrated intensity of a phase of interest (i.e. unhydrated MgO or uncarbonated $Mg(OH)_2$) to that of a standard phase introduced in the sample in a known proportion, was applied for the quantitative analysis of the phases present after the carbonation process. The internal standard used for quantification purposes was fluorite (CaF_2) included at 5 wt.% [23]. The RIR of the phases of interest was obtained by dividing the integrated intensity of the strongest line of each phase with that of the standard. As most HMC phases that form in carbonated RMC systems have overlapping peaks, their direct quantification presents a challenge. Therefore, the extent of hydration and carbonation within RMC samples can be calculated backwards by using the amounts of residual (i.e. unhydrated/uncarbonated) MgO and $Mg(OH)_2$. Calibration curves for MgO and $Mg(OH)_2$, the two main components used for quantitative analysis, are straight lines through

the origin i.e. y= kx, where x is the RIR of the phase analyzed and y is the weight fraction of the component investigated. The value of k is 0.2886 for MgO and 0.3651 for $Mg(OH)_2$ [3]. The RIR was acquired by dividing the integrated intensity of the strongest line of the phase with that of the standard.

TGA was conducted on a Perkin Elmer TGA 4000 equipment from 50 to 950 ^oC with a heating rate of 10 ^oC/min under nitrogen flow. SEM was carried out with a Zeiss Evo 50 microscope to investigate the morphologies of the hydration and carbonation products within the prepared samples. The vacuum dried samples were mounted onto aluminum stubs using double-sided adhesive carbon disks and coated with gold before SEM analysis. Along with SEM, BSE images were used to provide a quantitative analysis of the hydration and carbonation products. In preparation for BSE, the vacuum dried samples were mounted in epoxy resin for 24 hours and then ground and polished to obtain smooth surfaces. Sand paper was used prior to final polishing by diamond slurry with sizes of 9, 3 and 0.3 μm. Dust and diamond particles generated during the polishing process were removed by exposing the samples to an ultrasonic bath for 10 minutes, which was followed by 24 hours in vacuum and coating with gold prior to analysis.

3 Results

3.1 Isothermal calorimetry

Fig. 2 (a) and (b) present the heat flow and the cumulative heat of RMC pastes during the first 24 hours of hydration, respectively. The results indicated that the dissolution-nucleation

of MgO occurred a few minutes after mixing for all samples. The higher exothermal peaks and increased total heat outputs demonstrated by HA samples in comparison to the corresponding H_2O samples confirmed the active role of HA ($(CH_3COO)_2Mg$) in promoting the dissolution of MgO.

The introduction of seeds in both the H_2O and HA samples was effective in facilitating the hydration of MgO at early stages (~2-5 hours) through the provision of additional nucleation sites within the pore space. The higher and wider hydration peaks of the seeded samples demonstrated the enhancement of hydration via the introduction of seeds. As the use of HA also promoted hydration by leading to the precipitation of brucite away from the original MgO grains, the effect of seeding on early hydration was more obvious in H_2O than HA samples. The initially rapid hydration in seeded samples was followed by a relatively slower reaction when compared to the corresponding unseeded samples.

3.2 Water absorption

Table 3 lists the water absorption values of all samples after 14 and 28 days of carbonation curing. The significant decrease in the water absorption of all samples from 14 to 28 days of curing indicated the reduction in the amount of connected pores, which were filled by hydration and carbonation products. HA samples achieved 44-57% lower water absorption than the corresponding H_2O samples at both ages. The lower water absorption of HA samples could be attributed to the enhancement of hydration, which led to an improvement in HMC formation and sample microstructures via the increased availability of $Mg(OH)_{2(aq,s)}$ for carbonation.

When compared with the H_2O.S0 sample, the introduction of seeds reduced the water absorption by up to 39%. Amongst the H_2O samples that did not include any HA, water absorption decreased with an increase in seed content. The reduction in the water absorption values of the seeded samples were linked with the decrease in sample porosities via the enhanced nucleation and growth of hydrate and carbonate phases enabled by the introduction of seeds within the pore space. A similar trend was observed in seeded HA samples after 14 days of carbonation as the introduction of seeds reduced the amount of absorbed water by up to 30%. However, the use of seeds did not have any influence in reducing the water absorption values recorded at 28 days. The reduction of water absorption within seeded HA samples at 14 days could be attributed to the role of seeds in accelerating the nucleation and growth of brucite and the subsequent formation of carbonate phases at early ages.

3.3 Compressive strength

The compressive strength development of all concrete samples cured for up to 28 days is shown in Fig. 3. All samples demonstrated an increase in strength with time, which was an indication of the continuous formation of HMCs over the 28 days of curing. The initially rapid strength gain observed during the first 14 days was followed by a slower rate associated with the reduction in the rates of the hydration and carbonation reactions over time. Amongst all the prepared samples, the inclusion of seeds and/or HA significantly improved compressive strength, which was especially notable at ≥ 14 days of curing.

When compared to the control sample (H_2O.S0), the inclusion of HA (i.e. without any seed) led to 119% and 48% increase in the compressive strength of the HA.S0 sample after 3 and 7 days of curing, respectively. As carbonation proceeded, the compressive strength of HA.S0 reached 68 MPa at 28 days, which was 42% higher than the equivalent strength of H_2O.S0. The improvement of compressive strength in the presence of HA was attributed to the active role of HA in the enhancement of the hydration process, which led to the production of higher amounts of $Mg(OH)_{2(aq,s)}$ available for the subsequent carbonation reaction and thereby higher degrees of HMC formation.

The use of seeding (i.e. without any HA) also led to improved performance as evident by the compressive strengths of the H_2O.S0.5 and H_2O.S1.0 samples, which were up to 36% and 33% higher than the corresponding strengths of H_2O.S0 at 14 and 28 days, respectively. The positive contribution of seeds to the strength development of H_2O.S0.5 and H_2O.S1.0 was an indication of the active role of seeding in stimulating the nucleation of hydration and carbonation products away from the original MgO particles within the pore space. This improved arrangement of particles facilitated the creation of extra contact surface area for further hydration and carbonation within these samples. Unlike the introduction of seeds in PC and alkali-activated slag systems, which demonstrated accelerated hydration and strength gain at early ages [16, 17], the use of seeds improved the performance of RMC formulations mainly after 14 days of curing.

The simultaneous inclusion of HA and seeding within the HA.S0.5 sample outperformed all other samples after 7 days of curing. The plateau observed in the strength development of HA.S0 and HA.S1.0 between 7 and 14 days was replaced by a continuous strength gain in HA.S0.5. The compressive strengths of HA.S0.5 were 64% (59 vs. 36 MPa) and 46% (70 vs.

48 MPa) higher than those of the control sample at 14 and 28 days, respectively. This notable improvement in the performance of HA.S0.5 clearly proved the important roles of HA in enhancing the hydration of MgO and seeds in (i) stimulating the nucleation of the hydration and carbonation products away from the original grains to facilitate the further continuation of these reactions and (ii) acting as micro-aggregates that filled in the pore space. As shown by the differences in the strength development of all samples presented in Fig. 3, the use of HA and seeding in HA.S0.5 did not only lead to significant improvements in mechanical performance but also reduced the total curing time required to achieve a certain strength, thereby reducing the overall costs associated with sample preparation. Increasing the seed content from 0.5 to 1% within the HA.S1.0 sample led to similar strengths as other HA samples at 28 days, showing that any increase in seed usage beyond 0.5% did not provide a clear benefit in terms of mechanical performance.

3.4 XRD

The XRD patterns of all samples after 14 days of carbonation are shown in Fig. 4. All samples demonstrated the formation of various HMC phases due to carbonation, namely nesquehonite, dypingite and hydromagnesite. Along with HMCs, the presence of unhydrated MgO (main peak at 42.9° 2θ) and uncarbonated brucite (main peak at 38.1° 2θ) was observed in all samples with or without HA and/or seeds. The quantification of unhydrated MgO and uncarbonated brucite within all samples after 14 days of carbonation, as reported in Table 4, was performed with respect to the introduced fluorite (main peak at 28.2° 2θ).

When compared to the control sample (H_2O.S0), the use of HA in HA.S0 reduced the unhydrated MgO content from 43 to 34%. A similar trend reflecting a decrease in the MgO content was also seen with the introduction of seeds. These samples revealed higher hydration degrees than the control sample, which was reflected by the lower residual MgO contents of H_2O.S0.5 (37%) and H_2O.S1.0 (34%) when compared to H_2O.S0 (43%). Similar to the introduction of HA, the use of seeds increased the utilization of RMC by up to 19%. Furthermore, the simultaneous inclusion of HA and seeds resulted in the lowest residual MgO contents as revealed by samples HA.S0.5 (33%) and HA.S1.0 (31%), which translated into an increase in the utilization of RMC by up to 26%.

The inclusion of HA and/or seeds not only reduced the amount of residual MgO and therefore achieved higher hydration degrees, but also significantly reduced the uncarbonated brucite content when compared to the control sample. Accordingly, the use of HA in the HA.S0 sample reduced the uncarbonated brucite content of the control sample (H_2O.S0) from 53% to 33%, while the inclusion of seeds within the samples H_2O.S0.5 and H_2O.S1.0 led to values as low as 30%. The lower brucite contents revealed by samples containing HA and/or seeds indicated the role of these additives in improving carbonation, which could explain the higher compressive strengths of these samples than those of the control sample. While the presence of HA produced a bulk brucite structure to facilitate the diffusion of CO_2 and its reaction with Mg-bearing phases, the dispersion of seeds in the pore space enabled the formation of brucite on seed surfaces in addition to the surface of the MgO grains, thereby increasing the reactive surface area of brucite for carbonation. A slightly different scenario was observed in HA samples that incorporated seeds. As the use of HA led to the migration of complex magnesia-acetate ions away from their original particles to form a bulk brucite structure in the pore space regardless of the presence of seeds, the introduction of seeds stimulated the nucleation

process rather than extending the surface area of the bulk brucite for carbonation. As a result, seeds were not influential in reducing the uncarbonated brucite contents within HA.S0.5 and HA.S1.0 and led to similar values to those of HA.S0.

3.5 TGA

The mass loss and heat flow results of all samples after 14 days of carbonation are shown in Fig. 5. The two endothermic peaks corresponding to the dehydration of water bonded to HMCs were observed at 120 and 220 °C. A strong endothermic peak responsible for the decomposition of uncarbonated brucite, accompanied with the dehydroxylation (e.g. hydromagnesite) and decarbonation (e.g. nesquehonite) of HMCs was observed at around ~370-420 °C. This was followed by a broader peak corresponding to the decarbonation of HMCs at ~720 °C. The three main decomposition steps of all samples were consistent with the patterns presented in previous studies [24-30] and summarized as below:

50 to 300 °C: Dehydration of water bonded to HMCs (e.g. nesquehonite, hydromagnesite and dypingite), as shown in Equation 6 [24, 26-30].

$$xMgCO_3 \cdot yMg(OH)_2 \cdot zH_2O \rightarrow xMgCO_3 \cdot yMg(OH)_2 + zH_2O \quad (6)$$

300 to 500 °C: Decomposition of uncarbonated brucite (Equation 7), dehydroxylation of HMCs such as hydromagnesite and dypingite (Equation 8) and decarbonation of HMCs such as nesquehonite (Equation 9) [25-27, 29, 30].

$$Mg(OH)_2 \rightarrow MgO + H_2O \quad (7)$$

$$xMgCO_3 \cdot yMg(OH)_2 \rightarrow xMgCO_3 + yMgO + yH_2O \quad (8)$$

$$MgCO_3 \rightarrow MgO + CO_2 \quad (9)$$

500 to 900 °C: Decarbonation of HMCs, as shown in Equation 9 [27, 30].

The mass loss values observed at each step, along with the total mass loss, which represented the content of hydrate and carbonate phases within each sample, are listed in Table 5. A majority of the mass loss in all samples was recorded in the 300-500 °C temperature range, which was associated with several reactions involving the decomposition of uncarbonated brucite and the dehydroxylation and decarbonation of various HMCs. Differentiation between the mass loss due to the decomposition of HMCs and that of brucite was made by subtracting the mass loss due to the decomposition of uncarbonated brucite (i.e. calculated from the brucite content in Table 4) from the total mass loss.

In line with the XRD results, the introduction of HA led to improvements in the carbonation of RMC samples, which could be observed via a comparison of HA.S0 with the control sample (H_2O.S0). The mass loss due to the decomposition of HMCs within these samples increased by 31% with the use of HA. The inclusion of 0.5 and 1% seeds also led to enhanced carbonation within H_2O.S0.5 and H_2O.S1.0 samples, which was reflected by an up to 45% increase in the mass loss due to HMCs within these samples when compared to the control sample. These mass loss values included the decomposition of the small amount of seeds in addition to the carbonate phases that formed during the curing process. Although the

simultaneous inclusion of HA and seeds also revealed up to 38% higher mass losses associated with HMCs than the control sample, their contribution in enhancing the carbonate content was not much higher than samples involving the sole use of HA or seeds. These findings were consistent with the uncarbonated brucite contents calculated via XRD analysis in Section 3.4, revealing variations in the role of seeds depending on the presence of HA. In general, the lower unhydrated MgO contents, coupled with the higher degree of carbonate formation demonstrated by the phase quantification results, confirmed the notable contribution of HA and seeds in improving the hydration and carbonation capability of RMC formulations.

3.6 CO_2 sequestration

The improvements in the amount of CO_2 absorbed by each sample incorporating the use of HA and/or seeds were demonstrated through the quantification of the CO_2 sequestration ratio (R_{CO2}), which was calculated as shown in Equation 10, where P_{CO2} is the percentage of CO_2 sequestered (i.e. obtained by subtracting the mass loss associated with the loss of H_2O from the total mass loss between 300 and 900 °C) and P_{RMC} is the percentage of final mass at 900 °C (i.e. residual MgO). These figures involved the slight mass loss due to the decomposition of seeds during thermal analysis.

$$R_{CO2} = P_{CO2} / P_{RMC} \quad (10)$$

The results listed in Table 5 indicated that the addition of seeds increased the CO_2 sequestration ratio of the control sample by up to 96%, which increased with increasing seed

content. Similar to the use of seeds, the inclusion of HA without any seeds in sample HA.S0 improved the CO_2 sequestration of the control sample by 54%. The simultaneous inclusion of HA and seeds did not have a major influence on the CO_2 sequestration, as demonstrated by a comparison of samples HA.S0.5 and HA.S1.0 with HA.S0. This was because the use of HA led to the formation of a bulk brucite structure in the pore space, while the introduction of seeds stimulated the nucleation process rather than extending the surface area of the bulk brucite for carbonation. The increased CO_2 sequestration of samples including HA/seeds enabled a more extensive formation of HMCs that filled up the pore space and established a strong network, which was also evident from the significantly reduced water absorption values (Table 3) and higher compressive strength results (Fig. 3).

3.7 Microstructural analysis

Fig. 6 shows the BSE images of selected samples after 14 days of carbonation. As can be seen from these images, the hydration and carbonation products mostly formed on the surface of MgO particles (~30-40 μm). The porous structure of the control sample (H_2O.S0), in which large pore spaces (> 10 μm) were observed (Fig. 6 (a)), differed from the other samples. In contrast, the inclusion of seeds and HA individually led to denser microstructures with smaller pore spaces (< 4 μm) in samples H_2O.S0.5 (Fig. 6 (b)) and HA.S0 (Fig. 6 (c)), respectively. The hydration and carbonation products surrounding the spherical seeds (diameter of ~2-5 μm) within sample H_2O.S0.5 shown in Fig. 6 (b) proved the role of seeds in enabling the nucleation of brucite away from the original MgO particles and extending the amount of contact surface area between brucite and the diffused CO_2. On the other hand, when compared to the control sample, the increased formation of hydrate and carbonate

phases within the pore space in addition to the surface of MgO particles confirmed the role of HA in promoting the dissolution of MgO and leading to the formation of hydration products with a bulk structure within sample HA.S0 shown in Fig. 6 (c). The increase in the extent of hydration and carbonation associated with the use of seeds and HA led to unhydrated MgO particles with smaller sizes (< 10 μm) as well as diminished pore spaces (< 4 μm). The simultaneous use of seeds and HA within sample HA.S0.5 shown in Fig. 6 (d) revealed the densest microstructure amongst all samples, which contained the smallest amount of pores (< 3 μm). This reduction in the amount of pore space within sample HA.S0.5 was in line with its mechanical performance and phase quantification results presented earlier.

Fig. 7 and Fig. 8 reveal the morphology of H_2O and HA samples after 14 days of carbonation, respectively. Needle-like nesquehonite and disk/rose-like hydromagnesite/dypingite, which are the main sources of strength development in RMC formulations, were observed in all samples. The disk- or rose-like hydromagnesite/dypingite crystals that formed due to the carbonation process could be distinguished from the hydromagnesite seeds included within the initial mix, which possessed a round ball-like morphology, as indicated earlier in Fig. 1. HA samples generally presented dense microstructures with firmly blended nesquehonite layers, whereas a mix of hydromagnesite/dypingite along with nesquehonite needles were observed within H_2O samples. The dense microstructures generated by the use of HA could be associated with the role of HA in enhancing the hydration and subsequent carbonation reactions, thereby increasing the formation of carbonate phases.

The unseeded samples H_2O.S0 and HA.S0 (Fig. 7 (a) and Fig. 8 (a)) showed similar microstructures composed of carbonates with identical morphologies. In these samples, agglomeration of hydromagnesite/dypingite disks in a rose-like form with a diameter of ~1.5-

2 μm was observed to grow on the surface of nesquehonite needles with a diameter of ~1 μm. The use of HA enabled the formation of firmly bonded nesquehonite needles that led to the densification of the microstructure. The inclusion of seeds to provide additional nucleation sites for the formation of carbonate phases resulted in variations in the morphologies of HMCs and the overall microstructures of H_2O and HA samples when compared to those of the unseeded samples. The role of seeds in providing nucleation sites for the formation of HMCs was observed in H_2O.S0.5, H_2O.S1.0, HA.S0.5 and HA.S1.0 samples including 0.5-1% of seeds. In addition to the carbonate phases that formed as a result of the curing process, round hydromagnesite seeds with a diameter of ~1-6 μm (Fig. 1) were observed within the seeded samples.

While the absence of HA in sample H_2O.S0.5 revealed the formation of disk-like hydromagnesite/dypingite with a diameter of ~1.5-2 μm along with nesquehonite needles surrounding the seed particles (Fig. 7 (b)), the introduction of HA in sample HA.S0.5 (i.e. involving the simultaneous use of HA and seeds) led to the formation of large nesquehonite needles that nucleated and grew on the seed surfaces dispersed within the pore space (Fig. 8 (b)). The vast formation of large nesquehonite crystals within this sample was facilitated via the use of seeds that established a bond between these carbonates, thereby enabling the densification of the microstructure via the formation of nesquehonite “plates”, which were a combination of individual needles. In addition to their active role in stimulating the formation of HMCs by providing additional nucleation sites, the seed particles served as micro-aggregates that filled in the initially available pore space. These improvements in the microstructure could explain the improved mechanical performance of samples involving the use of HA and seeds.

Increasing the seed content to 1% in sample H_2O.S1.0 led to the dense formation of nesquehonite, which reduced the overall porosity. The presence of seeds was obvious from the widely observed seed particles, with diameters of ~6 μm, on top of the nesquehonite needles (Fig. 7 (c)). As observed earlier, the introduction of seeds in the pore space enhanced the overall carbonation process by providing extra surface for the continuation of the reaction and induced a filling effect that increased the overall density via their functioning as micro-aggregates amongst the carbonate crystals. These observations were in line with the reduction in the water absorption values and increase in the strength of H_2O samples with the introduction of seeding. Alternatively, increasing the seed content to 1% in sample HA.S1.0 demonstrated an excessive presence of seeds, with diameters of ~1-2 μm, partially covering the nesquehonite needles (Fig. 8 (c)). This could be due to the reduction in the available pore space via the higher degree of brucite formation within HA samples, thereby leaving a limited area for the dispersion of seeds throughout the sample microstructure. Within these constraints, the excessive usage of seeds, which themselves have limited bonding properties, may have led to the reduction of the bonding strength between the carbonate phases and aggregates, thereby explaining the lower strengths of HA.S1.0 when compared to HA.S0.5 after 14 days of carbonation.

4 Conclusions

In RMC-based concrete formulations, the formation of an initial layer of hydrates and/or carbonates can slow down the continuation of hydration and carbonation by establishing a physical barrier that prevents further contact between unreacted $MgO/Mg(OH)_2$ with H_2O/CO_2. These limitations can result in large amounts of unreacted MgO and $Mg(OH)_2$,

548 which translate into relatively low strength gain and porous microstructures. This study
549 aimed to improve the hydration, carbonation and associated mechanical performance of
550 RMC-based concrete formulations. This was achieved via the enhancement of the hydration
551 process through the use of a HA (magnesium acetate, $(CH_3COO)_2Mg$ at a concentration of
552 0.05 M) and the improvement of carbonation through the inclusion of carbonate seeds. The
553 prepared samples were subjected to carbonation under a CO_2 concentration of 10% for up to
554 28 days and tested for their water absorption, compressive strength, reaction degree, phase
555 formations as well as microstructural development. The overall results indicated that the
556 addition of HA and/or seeds significantly improved the hydration, carbonation and strength
557 of RMC-based concrete samples.
558
559 The main contribution of the presence of HA was its role in promoting the dissolution of
560 MgO and increasing the formation of hydration products with a bulk structure. This
561 improvement in the hydration process translated into higher amounts of well dispersed
562 brucite available for carbonation within the pore space. The introduction of seeds not only
563 enabled the nucleation of brucite away from the original MgO particles, but also extended the
564 amount of contact surface area between the Mg-phases and diffused CO_2. Moreover, seeds
565 acted as micro-aggregates that filled the pore space and enabled the vast formation of firmly
566 bonded large nesquehonite crystals, whose combination established dense carbonate clusters.
567 These improvements led to an increased utilization rate of RMC via enhanced hydration and
568 carbonation reactions.
569
570 The increase in the carbonation degree, coupled with the densification of the microstructure
571 via the formation of a strong network composed of large carbonate crystals with improved
572 morphologies, facilitated the strength development of RMC formulations involving the use of

HA and/or seeds. The enhancement of the reaction degrees was reflected as 28-day water absorption values as low as 0.85% (i.e. 56% lower than the control sample) and strengths as high as 70 MPa (i.e. 46% higher than the control sample). Therefore, the introduction of HA and seeding not only significantly increased the compressive strength of concrete mixes by increasing their CO_2 sequestration capabilities, but also enabled reduced material usage and shorter curing durations by improving the utilization degree of RMC and facilitating early strength development.

Acknowledgement

The authors would like to acknowledge the financial support from the Singapore MOE Academic Research Fund Tier 1 (RG 113/14) for the completion of this research project.

References

[1] J. Green, Calcination of precipitated Mg(OH)2 to active MgO in the production of refractory and chemical grade MgO, Journal of Materials Science, 18 (1983) 637-651.

[2] V.S.S. Birchal, S.D.F. Rocha, V.S.T. Ciminelli, The effect of magnesite calcination conditions on magnesia hydration, Minerals Engineering, 13 (2000) 1629-1633.

[3] M. Liska, A. Al-Tabbaa, Ultra-green construction: reactive magnesia masonry products, Proceedings of the Institution of Civil Engineers - Waste and Resource Management, 162 (2009) 185-196.

[4] R.L. Frost, S. Bahfenne, J. Graham, W.N. Martens, Thermal stability of artinite, dypingite and brugnatellite—Implications for the geosequestration of green house gases, Thermochimica Acta, 475 (2008) 39-43.

[5] A.V. Saetta, B.A. Schrefler, R.V. Vitaliani, 2 — D model for carbonation and moisture/heat flow in porous materials, Cement and Concrete Research, 25 (1995) 1703-1712.

[6] L.F. Amaral, I.R. Oliveira, R. Salomão, E. Frollini, V.C. Pandolfelli, Temperature and common-ion effect on magnesium oxide (MgO) hydration, Ceramics International, 36 (2010) 1047-1054.

[7] S.D.F. Rocha, M.B. Mansur, V.S.T. Ciminelli, Kinetics and mechanistic analysis of caustic magnesia hydration, Journal of Chemical Technology & Biotechnology, 79 (2004) 816-821.

[8] C. Unluer, A. Al-Tabbaa, Enhancing the carbonation of MgO cement porous blocks through improved curing conditions, Cement and Concrete Research, 59 (2014) 55-65.

[9] F. Jin, A. Al-Tabbaa, Thermogravimetric study on the hydration of reactive magnesia and silica mixture at room temperature, Thermochimica Acta, 566 (2013) 162-168.

[10] V.S. Birchal, S.D.F. Rocha, M.B. Mansur, V.S.T. Ciminelli, A simplified mechanistic analysis of the hydration of magnesia, The Canadian Journal of Chemical Englneerlng, 79 (2001) 5.

[11] O. Fruhwirth, G.W. Herzog, I. Hollerer, A. Rachetti, Dissolution and hydration kinetics of MgO, Surface Technology, 24 (1985) 301-317.

[12] D.A. Vermilyea, The dissolution of MgO and $Mg(OH)_2$ in aqueous solutions, Journal of The Electrochemical Society, 116 (1969) 1179-1183.

620 [13] D. Filippou, N. Katiforis, N. Papassiopi, K. Adam, On the kinetics of magnesia
621 hydration in magnesium acetate solutions, Journal of Chemical Technology &
622 Biotechnology, 74 (1999) 322-328.
623 [14] K.P. Matabola, E.M. van der Merwe, C.A. Strydom, F.J.W. Labuschagne, The influence
624 of hydrating agents on the hydration of industrial magnesium oxide, Journal of Chemical
625 Technology & Biotechnology, 85 (2010) 1569-1574.
626 [15] C. Unluer, A. Al-Tabbaa, Impact of hydrated magnesium carbonate additives on the
627 carbonation of reactive MgO cements, Cement and Concrete Research, 54 (2013) 87-97.
628 [16] J.J. Thomas, H.M. Jennings, J.J. Chen, Influence of nucleation seeding on the hydration
629 mechanisms of tricalcium silicate and cement, The Journal of Physical Chemistry C, 113
630 (2009) 4327-4334.
631 [17] M.H. Hubler, J.J. Thomas, H.M. Jennings, Influence of nucleation seeding on the
632 hydration kinetics and compressive strength of alkali activated slag paste, Cement and
633 Concrete Research, 41 (2011) 842-846.
634 [18] M.A. Shand, The chemistry and technology of magnesia, John Wiley & Sons2006.
635 [19] ASTM C1702 − 15a, Standard test method for measurement of heat of hydration of
636 hydraulic cementitious materials using isothermal conduction calorimetry, ASTM Committee
637 C01, West Conshohocken, PA 19428-2959, United States, 2015, pp. 8.
638 [20] C.R. Hubbard, R.L. Snyder, RIR-measurement and use in quantitative XRD, Powder
639 Diffraction, 3 (1988) 74-77.
640 [21] R.L. Snyder, The use of reference intensity ratios in X-ray quantitative analysis, Powder
641 Diffraction, 7 (1992) 186-193.
642 [22] Q. Johnson, R. Zhou, Checking and estimating RIR values, Advances in X-ray Analysis,
643 42 (2000) 287-296.
644 [23] H.P. Klug, L.E. Alexander, X-ray diffraction procedures, (1954).

[24] V. Vágvölgyi, R.L. Frost, M. Hales, A. Locke, J. Kristóf, E. Horváth, Controlled rate thermal analysis of hydromagnesite, Journal of Thermal Analysis and Calorimetry, 92 (2008) 893-897.

[25] L.A. Hollingbery, T.R. Hull, The thermal decomposition of huntite and hydromagnesite—A review, Thermochimica Acta, 509 (2010) 1-11.

[26] R.L. Frost, S.J. Palmer, Infrared and infrared emission spectroscopy of nesquehonite Mg(OH)(HCO3)· 2H2O–implications for the formula of nesquehonite, Spectrochimica Acta Part A: Molecular and Biomolecular Spectroscopy, 78 (2011) 1255-1260.

[27] G. Jauffret, J. Morrison, F. Glasser, On the thermal decomposition of nesquehonite, Journal of Thermal Analysis and Calorimetry, 122 (2015) 601-609.

[28] S. Purwajanti, L. Zhou, Y. Ahmad Nor, J. Zhang, H. Zhang, X. Huang, C. Yu, Synthesis of magnesium oxide hierarchical microspheres: A dual-functional material for water remediation, ACS applied materials & interfaces, 7 (2015) 21278-21286.

[29] P. Ballirano, C. De Vito, V. Ferrini, S. Mignardi, The thermal behaviour and structural stability of nesquehonite, MgCO3·3H2O, evaluated by in situ laboratory parallel-beam X-ray powder diffraction: New constraints on CO2 sequestration within minerals, Journal of Hazardous Materials, 178 (2010) 522-528.

[30] R.L. Frost, S. Bahfenne, J. Graham, W.N. Martens, Thermal stability of artinite, dypingite and brugnatellite—Implications for the geosequestration of green house gases, Thermochimica Acta, 475 (2008) 39-43.

List of Tables

Table 1 Chemical composition and physical properties of RMC.

	Chemical composition (%)							Physical properties	
	MgO	SiO_2	CaO	R_2O_3	K_2O	Na_2O	LOI	Specific gravity (g/cm^3)	Specific surface area (m^2/g)
RMC	>91.5	2.0	1.6	1.0	-	-	4.0	3.0	16.3

Table 2 Compositions of concrete samples investigated in this study.

Mix label	Seed (%)	Mix proportion (kg)				
		RMC	Seed	Aggregates	H_2O	HA
H_2O.S0	0	500	0	1100	350	-
H_2O.S0.5	0.5	497.5	2.5		350	-
H_2O.S1.0	1.0	495	5		350	-
HA.S0	0	500	0		-	350
HA.S0.5	0.5	497.5	2.5		-	350
HA.S1.0	1.0	495	5		-	350

Table 3 Water absorption of all samples after 14 and 28 days of curing.

Mix label	Water absorption (%)	
	14 days	28 days
H_2O.S0	4.12	1.95
H_2O.S0.5	3.29	1.84
H_2O.S1.0	2.53	1.66
HA.S0	2.01	0.83
HA.S0.5	1.75	0.85
HA.S1.0	1.41	0.86

Table 4 MgO and $Mg(OH)_2$ contents of all samples obtained by XRD after 14 days of curing.

Mix label	MgO (%)	Brucite (%)
H_2O.S0	43	53
H_2O.S0.5	37	44
H_2O.S1.0	34	30
HA.S0	34	33
HA.S0.5	33	34
HA.S1.0	31	35

Table 5 Mass loss and carbonation degrees of all samples obtained by TGA after 14 days of curing.

Mix label	Mass loss (wt.%)						R_{CO2}
	50-300 °C	300-500 °C	500-900 °C	Brucite	HMCs	Total	
H_2O.S0	8.13	27.41	2.79	16.41	21.92	38.33	0.082
H_2O.S0.5	10.89	28.16	2.66	13.52	28.19	41.71	0.134
H_2O.S1.0	11.13	27.22	2.68	9.28	31.75	41.03	0.161
HA.S0	8.44	27.87	2.62	10.35	28.58	38.93	0.126
HA.S0.5	10.16	27.52	2.37	10.52	29.53	40.05	0.133
HA.S1.0	10.54	27.68	2.77	10.84	30.15	40.99	0.125

List of Figures

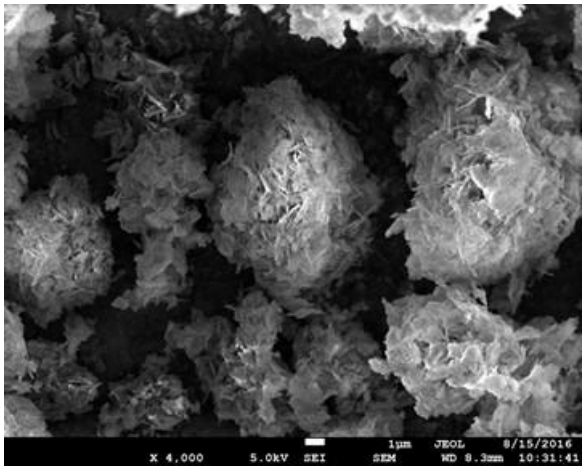

Fig. 1 SEM image of hydromagnesite seeds

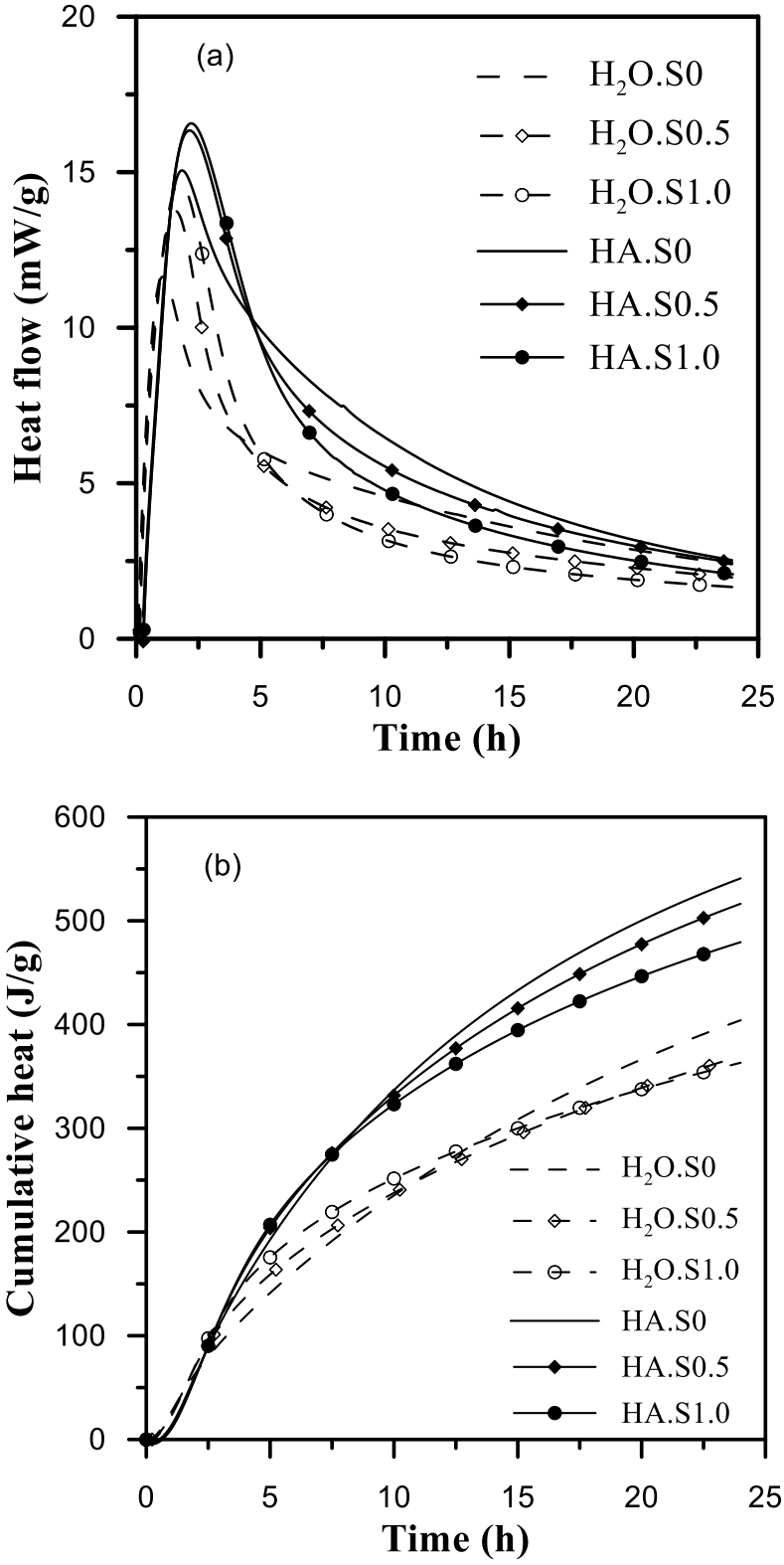

Fig. 2 Isothermal calorimetry results of pastes showing the (a) heat flow and (b) cumulative heat

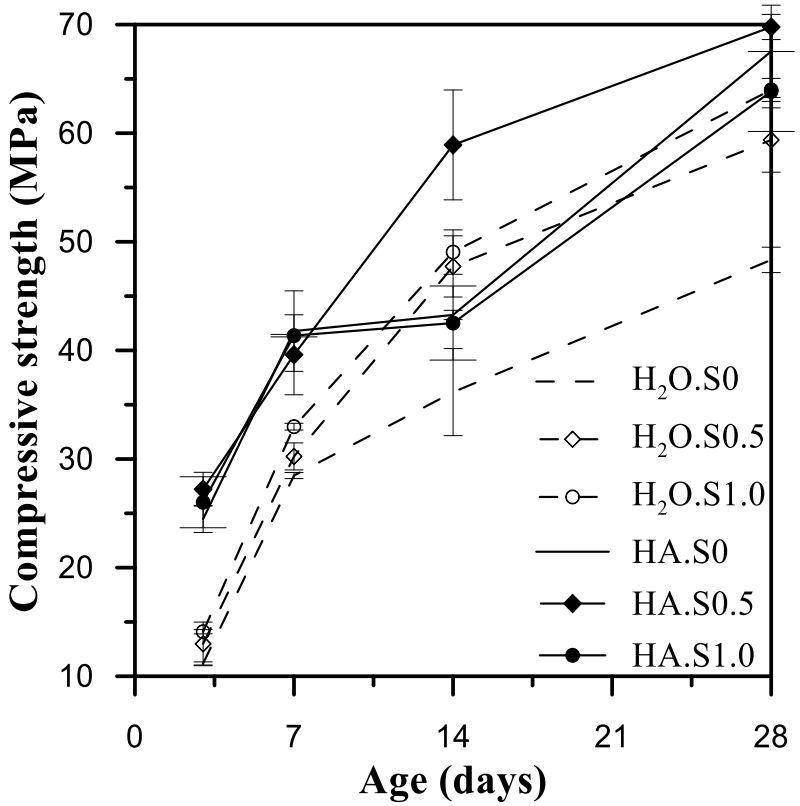

Fig. 3 Compressive strength of all samples cured for up to 28 days

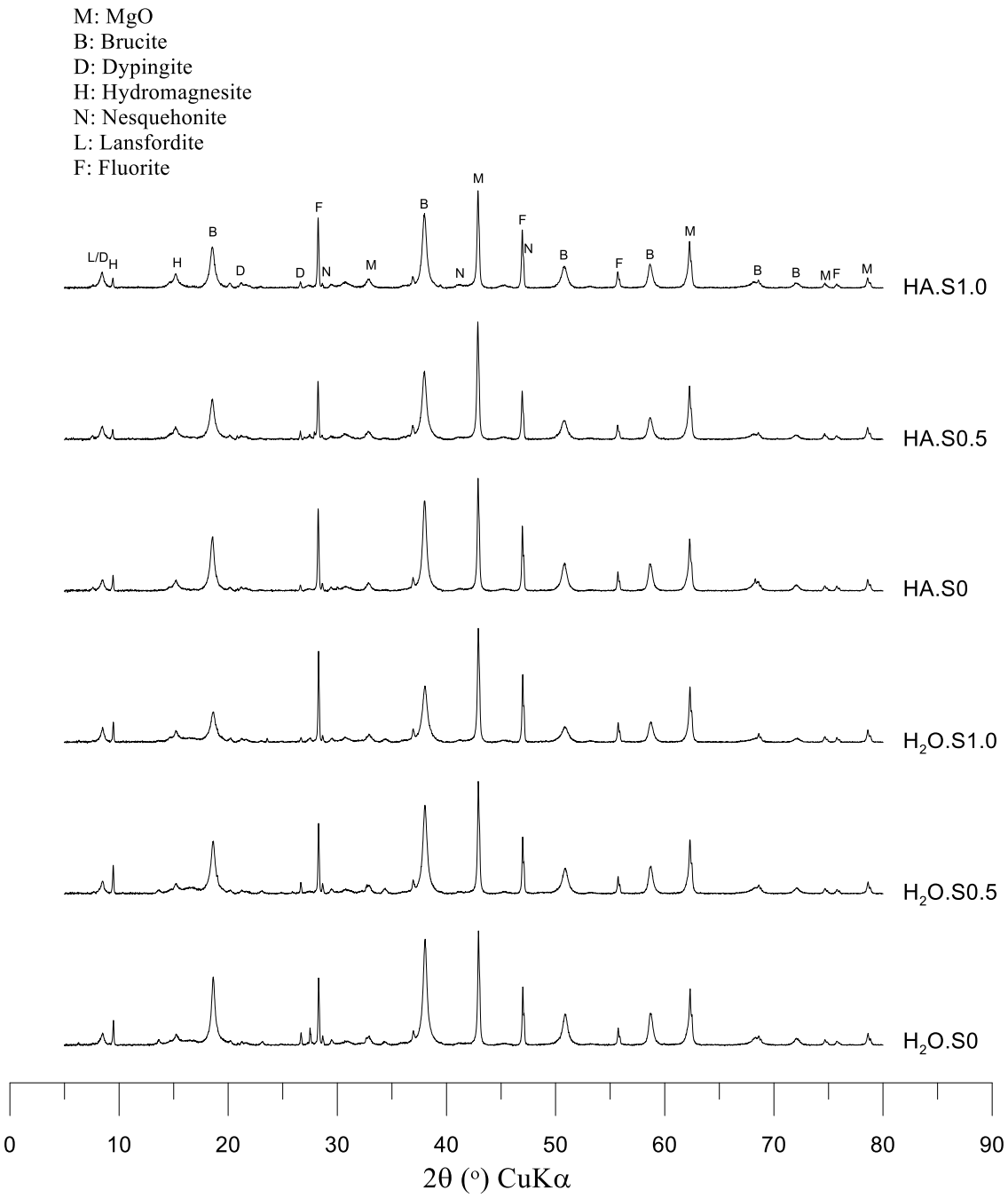

Fig. 4 XRD patterns of all samples after 14 days of curing

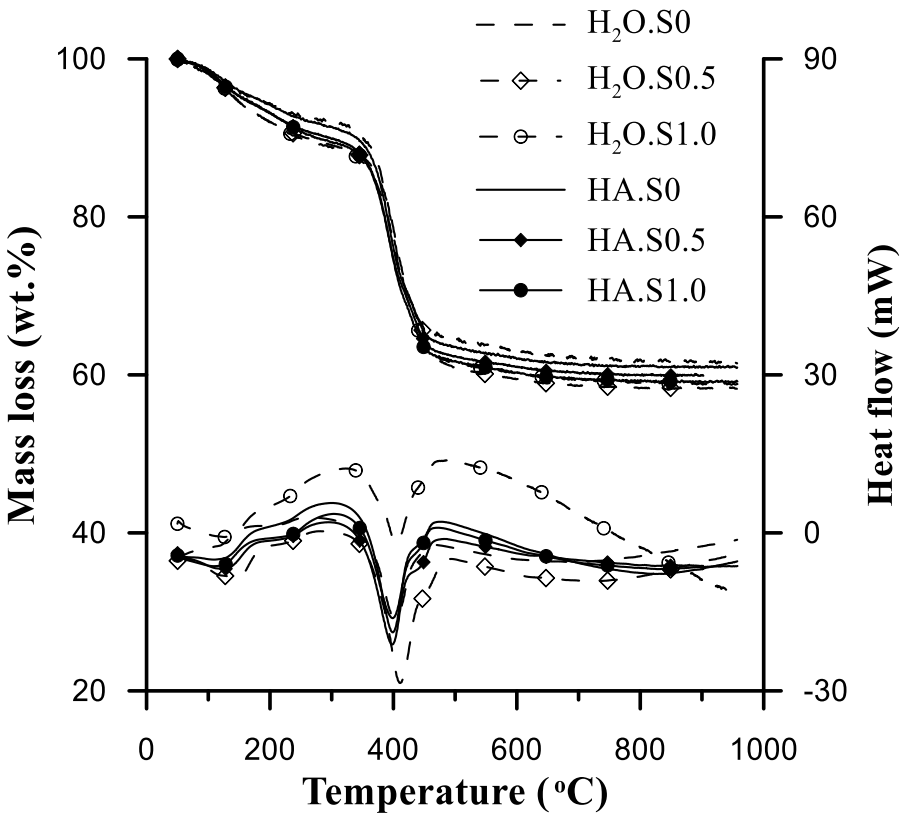

Fig. 5 Mass loss and heat flow of all samples after 14 days of curing

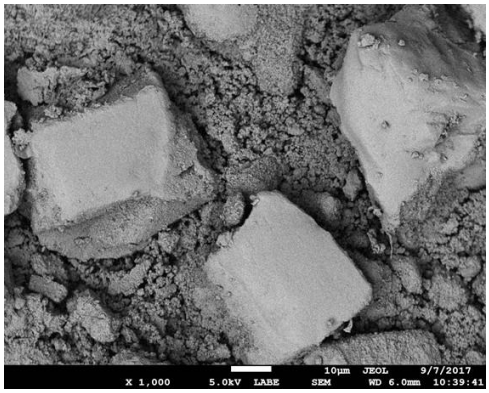

(a)

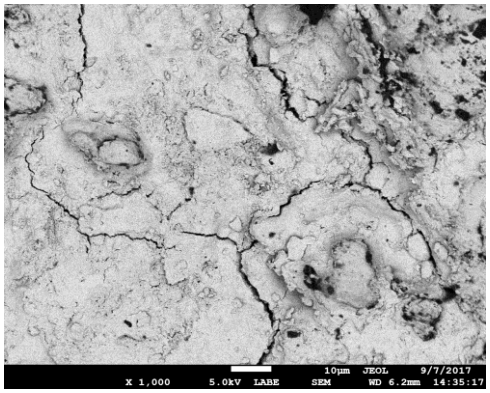

(b)

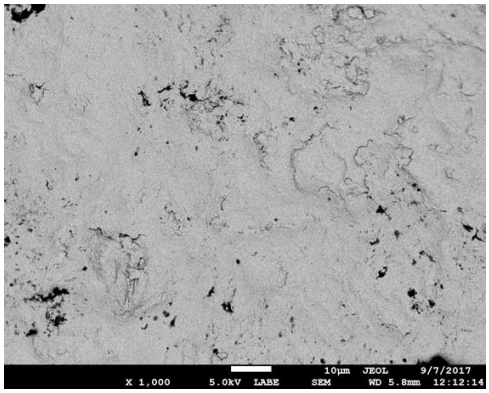

(c)

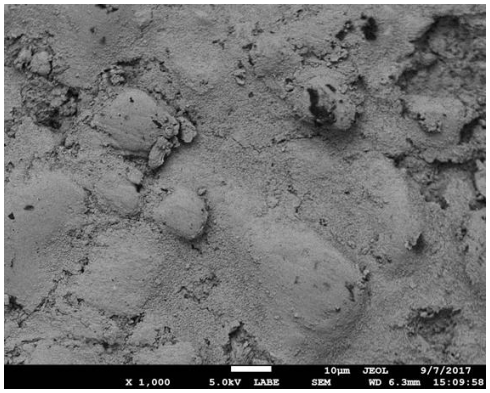

(d)

Fig. 6 BSE images of selected samples after 14 days of curing: (a) H_2O.S0, (b) H_2O.S0.5, (c) HA.S0 and (d) HA.S0.5

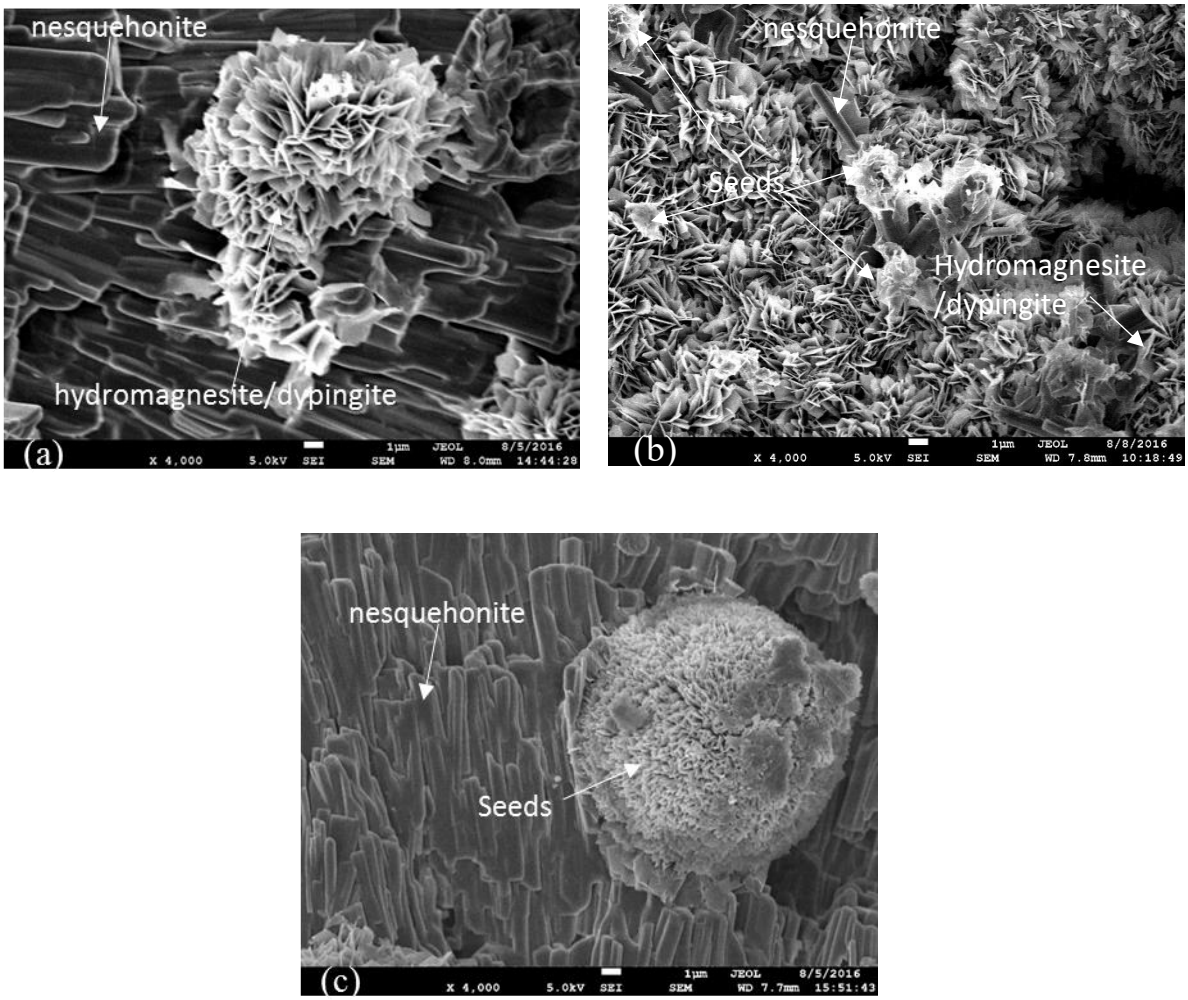

Fig. 7 SEM images of H_2O samples after 14 days of curing: (a) H_2O.S0, (b) H_2O.S0.5 and (c) H_2O.S1.0

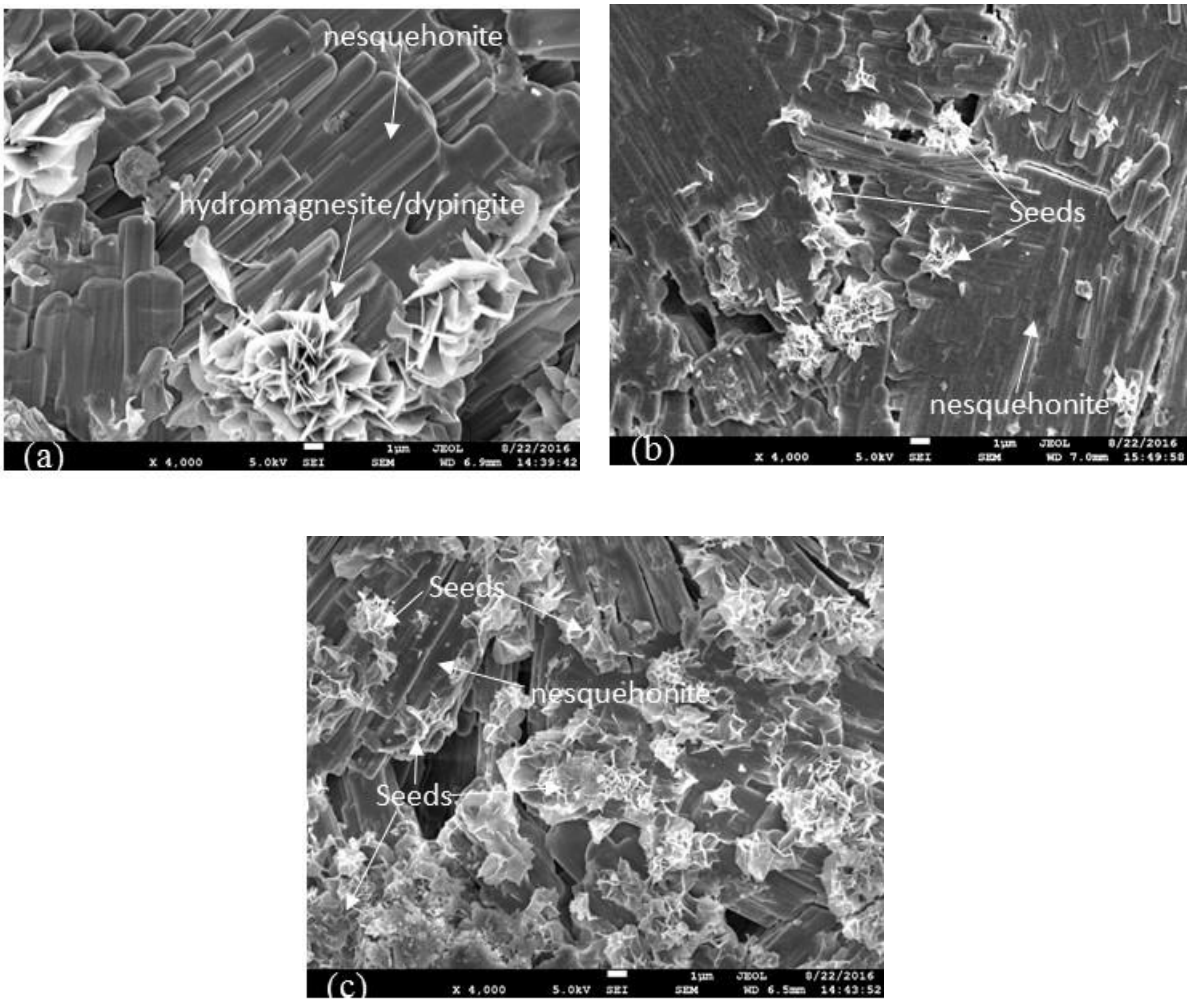

Fig. 8 SEM images of HA samples after 14 days of curing: (a) HA.S0, (b) HA.S0.5 and (c) HA.S1.0